Electron affinities and ionization energies of Cu and Ag delafossite compounds: A hybrid functional study

Mao-Sheng Miao, Sam Yarbro, Phillip T. Barton, and Ram Seshadri

Materials Department, Department of Chemistry and Biochemistry, and Materials Research Laboratory,
University of California, Santa Barbara, California 93106, USA
(Received 24 July 2013; revised manuscript received 22 December 2013; published 21 January 2014)

Using density functional theory with a hybrid functional, we calculate the ionization energies and electron affinities of a series of delafossite compounds (AMO$_2$: A = Cu, Ag; M = B, Al, Ga, In, Sc). The alignments of the valence band maximum and the conduction band minimum, which directly relate to the ionization energies and electron affinities, were obtained by calculations of supercell slab models constructed in a nonpolar orientation. Our calculations reveal that the ionization energy decreases with an increasing atomic number of group-III elements, and thus suggest an improved p-type doping propensity for heavier compounds. For keeping both a low ionization energy and a band gap of sufficient size, CuScO$_2$ is superior to the Cu-based group-III delafossites. By analyzing the electronic structures, we demonstrate that the compositional trend of the ionization energies and electron affinities is the result of a combined effect of d-band broadening due to Cu(Ag)-Cu(Ag) coupling and a repositioning of the d-band center.

I. INTRODUCTION

Transparent conducting oxides (TCOs) have attracted attention in the past few decades because of their application as current-spreading layers in optoelectronic devices such as solar cells and light emitting diodes. Special interest is paid toward the application for transparent electronics, however, such devices require complementary doping that has yet to be achieved on a functional level [1]. While n-type TCOs such as In$_{2-x}$Sn$_x$O$_3$ (ITO) find widespread use, p-type TCOs still remain elusive [2]. The difficulty of hole doping oxides comes from the fundamental limitation of their typical electronic structure. Oxides often possess large ionization energies (IEs) and electron affinities (EAs), which make them highly susceptible to n-type doping but extremely disinclined to p-type doping. Additionally, the valence band maximum (VBM) derives dominantly from O-$2p$ states and holes tend to localize on O^{2-}, limiting the hole mobilities.

One approach to improve p-type doping propensity is to mix $3d$ states into the valence band. Among the first-studied p-type TCOs, Cu$_2$O showed a strong potential because of its high d^{10} states that lead to a smaller ionization energy and allow hole doping. The p-type nature of the undoped sample is attributed to Cu vacancies and the corresponding Cu^{2+} state. Cu$_2$O also has a reasonable hole mobility, as high as 100 cm^2/V s. However, its small band gap, E_g = 2.1 eV, precludes the requisite transparency [3].

The mixing of Cu$_2$O with group-III oxides opens up a wider band gap by reducing the dimensionality from three dimensions (3D) to two dimensions (2D), while the ability to create mobile holes is retained. The corresponding delafossite materials have thus been examined closely as p-type TCOs, with the prototypical CuAlO$_2$ exhibiting E_g = 3.1 eV and high electrical conductivity [2,4,5]. The delafossite structure has long been of interest because it hosts both metallic and insulating behavior, as is well exemplified by the metal-insulator transition in a partial solid solution between AgNiO$_2$ and AgCoO$_2$ [6]. In the past decade, the search for p-type TCOs in the delafossite family has been expanded both by replacing Al with other trivalent metals and by substituting Ag for Cu. Promising improvements in the p-type conductivity are seen in doped CuScO$_2$ and CuCrO$_2$.

To investigate the nature of p-type conductivity, the electronic structures of many delafossites have been investigated by density functional theory (DFT) calculations, and particular interest has been paid to the Cu-containing p-type TCOs. Evidence has been obtained that the p-type conductivity originates from the formation of Cu vacancies and facile oxidation of Cu^{1+} to Cu^{2+} [7]. By calculating the band offsets using a superlattice model, Shi *et al*. found that CuScO$_2$ has a higher valence band maximum than group-III Cu-based delafossites [8]. More recently, Scanlon *et al*. discussed the conductivity anomalies in Cu-based delafossites and showed the importance of M-O bonding for conductivity [9]. In addition, the extent of M-M bonding in delafossites has been examined with DFT for a number of different A and B cations [10,11]. In these studies the authors note that both the A- and B-site cations contribute to the electronic structure near the Fermi level. They also found that the A-site d_{z^2} orbitals are responsible for the highly disperse bands and may be important for stabilizing metallic ground states.

Despite the many theoretical studies of the delafossites, both the doping propensity and the variation of conductivity within the family are not well understood while both cations are subject to replacement. The ionization energy and electron affinity can provide a general indication of the p- and n-type doping propensity of a material [12]. Generally speaking, a smaller ionization energy (or higher VBM position) facilitates p-type doping, while a larger electron affinity [lower conduction band minimum (CBM) position] tends to indicate ease of n-type doping.

The ionization energy and electron affinity of TCOs are also important in optoelectronic devices. They determine, for example, the work function of the TCO used in an organic photovoltaic (OPV), which plays a key role and can be tailored to optimize the device efficiency. These electronic properties have thus been rigorously studied for p-type TCOs. However, the work function is not a unique bulk property and can vary

with crystal orientation, surface/interface reconstruction, and strain [13]. The work function can also be greatly modified by the doping level.

The p-type doping of oxides is also important in the field of dilute magnetic semiconductors (DMSs) [14]. DMS materials have been realized in III-V and II-VI compounds where p-type doping is the key factor since the ferromagnetism originates from the hole-mediated coupling between local spins [15]. The hole doping can either come from single magnetic dopants or from codoping of a transition metal and p-type dopant. For either approach, the doping propensities can be revealed by the ionization energies and electron affinities.

Most previous studies employed local or semilocal functionals that are known to have discrepancies not only on the band gap but also on the alignment of band edge states. In this paper, we conduct a systematic study of the ionization energies and the electron affinities using a hybrid functional, for a series of Cu and Ag delafossite compounds AMO_2 (A = Cu, Ag; M = B, Al, Ga, In, Sc). By constructing supercells containing slabs that model the bulk and surface area of AMO_2, we calculated the values of the VBM and the CBM aligned to the vacuum. Trends in the EA and IE are discussed.

II. METHODOLOGY

The computational methods used here are based on density functional theory (DFT). The Vienna *ab initio* simulation package (VASP) is used throughout to perform the calculations, in which the wave functions are described a by plane-wave basis and the ionic potential is described by the projector augmented wave (PAW) approach. Both the Perdew-Burke-Ernzerhof (PBE) generalized gradient approximated (GGA) functionals and the Heyd-Scuseria-Ernzerhof (HSE) hybrid functionals are used for the exchange-correlation potentials and energies.

Using both PBE and HSE methods, we optimized the atomic structures of selected Cu and Ag delafossites (AMO_2, in which A = Cu, Ag and M = B, Al, Ga, In, Sc) and calculated the electronic structures. The calculations are done for a $2H$ structure. The unit cell used in the calculations is shown in Fig. 1(a). An $8 \times 8 \times 2$ Monkhorst-Pack k mesh is used for all the delafossite calculations. A cutoff energy of 550 eV is used for geometry relaxation, and 400 eV for electronic structure calculations such as band structure and density of states.

In order to determine the ionization energies and electron affinities, we use slab calculations to align the average electrostatic potential of the bulk delafossites with that of the vacuum. The slabs are constructed with four consecutive layers of Cu atoms and Al-O octahedra [Fig. 2(a)]. We construct the slabs in the nonpolar [1$\bar{1}$0] direction to eliminate the effect of surface dipoles. For Cu$_2$O and Ag$_2$O, the [1$\bar{1}$0] direction is slightly polarized, but much weaker than in the [100] direction. In-plane lattice constants are fixed at the bulk values and the atom positions in the two center layers are also frozen. The macroscopic average potential is obtained by first averaging the electrostatic potential on planes parallel to the surfaces and then averaging over a certain interplanar distance. This procedure removes all the atomic-scale oscillations of the potential and yields an electrostatic potential profile that
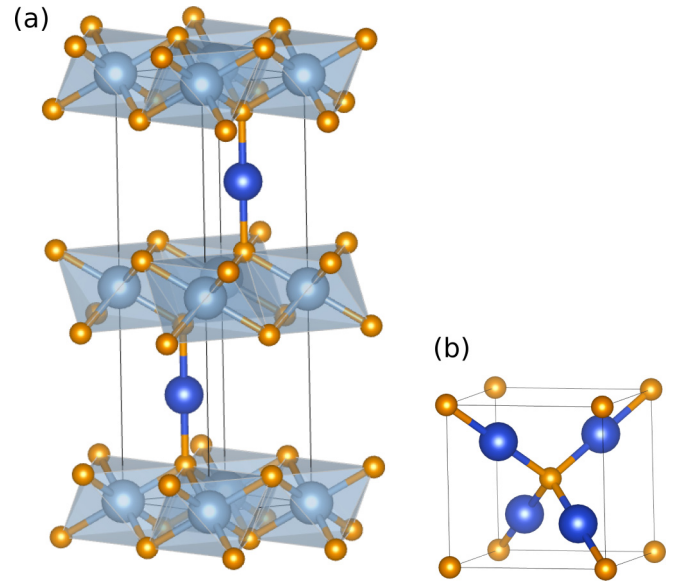

FIG. 1. (Color online) Crystal structures of (a) CuAlO$_2$ $2H$ delafossite and (b) Cu$_2$O. The reduced dimensionality of the delafossite structure widens its electronic band gap. Cu, Al, and O are shown in blue, gray, and orange.

unambiguously displays the potential difference Φ_{el} between the center of the bulk delafossites and the vacuum [Fig. 2(b)]. The ionization energy E_{IE} and electron affinity E_{EA} are calculated by

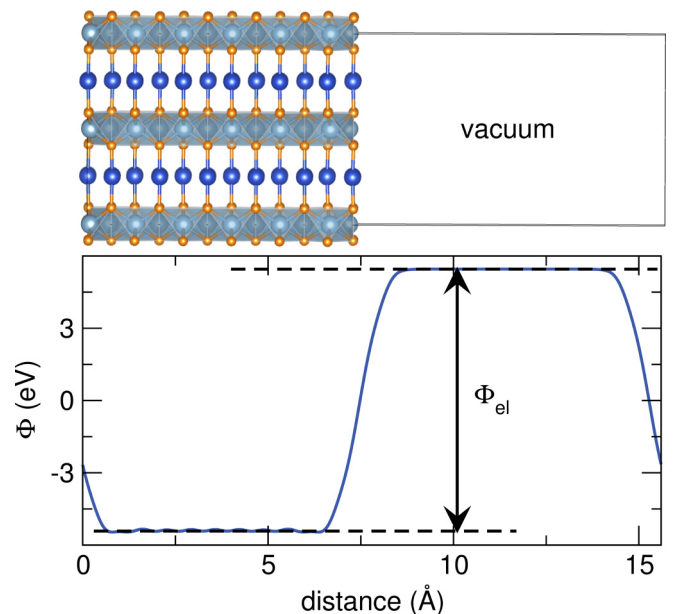$$E_{IE} = \Phi_{el} - E_{VBM}, \qquad E_{EA} = \Phi_{el} - E_{CBM}, \qquad (1)$$

FIG. 2. (Color online) A schematic slab model (top) and the corresponding profile of the calculated electrostatic potential (bottom). The difference between the potential within the slab and vacuum determines the absolute position of the band edges. These positions are directly related to the ionization energy and electron affinity, which enable the comparison and evaluation of delafossite materials as TCOs.

TABLE I. The lattice constants ($a = b$), c/a ratio, A-O (A = Cu, Ag), and M-O (M = B, Al, Ga, In, Sc) bond lengths for delafossite oxides. The parameters marked by * are taken from a $3R$ structure, since their $2H$ structures are not available. The c/a for these compounds are reduced proportionally from a three-layer $3R$ cell to a two-layer $2H$ cell. NA stands for not available.

	$a = b$ (Å)			c/a			A-O (Å)			M-O (Å)		
	PBE	HSE	Expt.	PBE	HSE	Expt.	PBE	HSE	Expt.	PBE	HSE	Expt.
Cu_2O	4.276	4.260	4.269 [17]	1	1	1	1.852	1.845	1.848	NA	NA	NA
$CuBO_2$	2.534	2.506	2.84 [18]	4.386	4.389	5.817 [18]	1.905	1.885		1.704	1.685	
$CuAlO_2$	2.873	2.847	2.863 [19]	3.969	3.968	3.951 [19]	1.880	1.863	1.866	1.921	1.904	1.913
$CuGaO_2$	3.001	2.978	2.977 [19]	3.830	3.837	3.845 [19]	1.868	1.857	1.848	2.013	1.989	1.996
$CuInO_2$	3.324	3.304	3.292 [20]*	3.526	3.514	3.521	1.846	1.868	1.848	2.204	1.908	2.174
$CuScO_2$	3.234	3.223	3.223 [19]	3.543	3.537	3.541	1.838	1.827	1.834	2.131	2.139	2.122
Ag_2O	4.828	4.827	4.723 [21]	1	1	1	2.091	2.090	2.045	NA	NA	NA
$AgBO_2$	2.638	2.612		4.597	4.578		2.173	2.173		1.749	1.749	
$AgAlO_2$	2.918	2.892	2.896 [22]	4.247	4.237	4.220	2.138	2.112	2.101	1.939	1.922	1.925
$AgGaO_2$	3.032	3.004		4.141	4.134		2.125	2.109		2.023	2.000	
$AgInO_2$	3.304	3.300	3.277 [23]*	3.866	3.833	3.841	2.102	2.026	2.078	2.198	2.201	2.173
$AgScO_2$	3.230	3.226	3.069 [24]*	3.867	3.856	4.039	2.097	2.091	2.126	2.129	2.120	2.021

in which E_{VBM} and E_{CBM} are the absolute values of the VBM and CBM energies obtained from bulk calculations. Although this method has been widely used in calculating the band edge states of various semiconductors, it can be limited by surface effects. The redistribution of charges and the presence of dipoles at the surface may slightly alter the electrostatic potential alignment of the bulk and vacuum regions. These surface effects are largely reduced by carefully choosing nonpolar surfaces and constraining the relaxation of the surface atoms, however, the effects cannot be totally diminished. The use of hybrid quantum mechanical/molecular mechanical calculations of the interface between the two compared materials may avoid the above problem and resolve band alignment to very high accuracy [16].

III. RESULTS

A. Crystal structure

The AMO_2 delafossite structure type ($CuFeO_2$, 1946) [25] consists of two types of cations, of which one is monovalent (A = Cu, Ag, Pd, Pt) and the other is trivalent (M = B, Al, Ga, In, Sc, Fe, Y, etc.). The trivalent cations form a continuous sheet of MO_6 octahedra. These stacked sheets of octahedra are connected by the monovalent A cations through linear O-A-O bonds [Fig. 1(a)]. Variation of sheet stacking leads to the $2H$ and $3R$ delafossite polytype structures. The $2H$ structure is in $P6_3/mmc$ space group (No. 194) and consists of two MO_6 layers per unit cell that are stacked in a similar way as in the hcp structure. The $3R$ structure contains three MO_6 layers per unit cell and exhibits rhombohedral symmetry of a space group of $R\bar{3}m$ (No. 166). The energy difference between the $2H$ and $3R$ polytypes is usually quite small for delafossites. For example, our PBE calculations for $CuAlO_2$ show that the $2H$ is only 16 meV higher in energy than the $3R$. In addition to the enthalpies of formation, the electronic structures of the two $CuAlO_2$ polytypes are also very similar, with the band gap of $2H$ only 0.04 eV larger than that of the $3R$. This is contrary to some other semiconductor materials such as SiC where the band gap differences can be as large as 1 eV [26,27]. Because the differences between the $2H$ and $3R$ polytypes are very small, we concentrate solely on the $2H$

TABLE II. The calculated band gaps for Cu_2O, Ag_2O, and selected delafossites. The experimental methods used are optical absorption spectroscopy, unless specifically denoted. UV-vis denotes UV visible diffuse reflectance spectrometry.

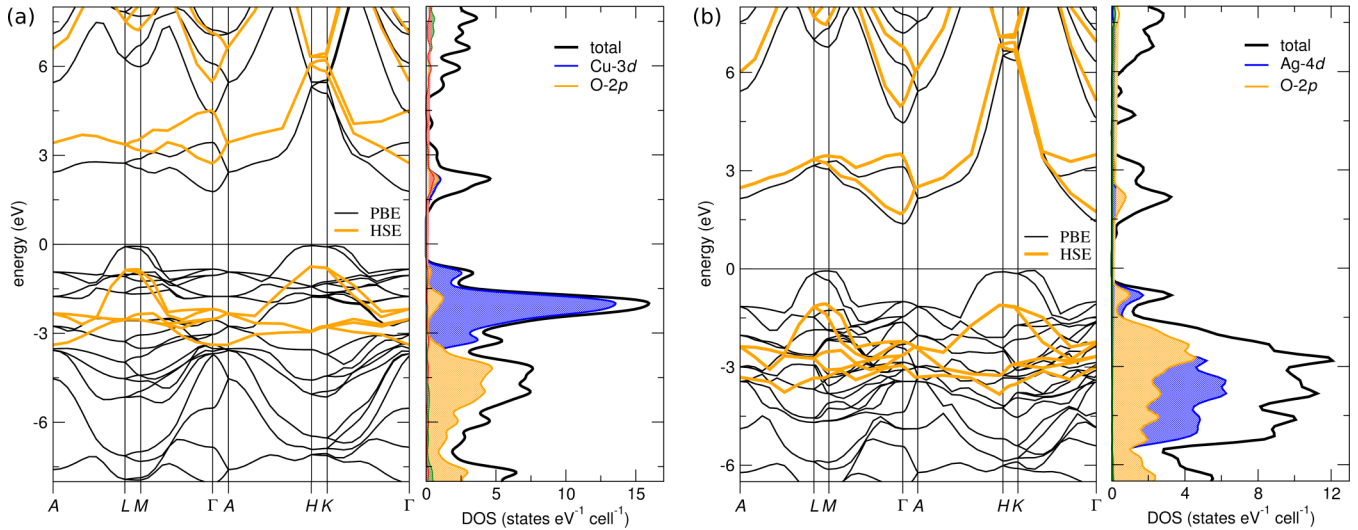|	E_g (eV)		
	PBE	HSE	Expt.
Cu_2O	0.522	2.030	2.1 ± 0.1 [28]
$CuBO_2$	1.549	3.195	3.1 [29] (DFT)
$CuAlO_2$	1.820	3.450	3.0 [30] (XPS)
$CuGaO_2$	0.802	2.427	3.6 [31], 3.7 [32]
$CuInO_2$	0.306	1.735	3.9 [33]
$CuScO_2$	2.690	4.053	4.24 [34] (XPS), 4.35 [35]
Ag_2O	-0.064	1.094	1.2 [36]
$AgBO_2$	0.731	1.967	
$AgAlO_2$	1.443	2.757	2.81 [37] (UV-vis), 2.95 [38] (UV-vis), 3.6 [39]
$AgGaO_2$	0.593	1.965	2.4 [40], 4.12 [41] (transmittance)
$AgInO_2$	0.290	1.655	1.90 [42]
$AgScO_2$	2.131	3.548	3.8 [39]

FIG. 3. (Color online) The electronic band structures (left panels) and projected densities of states (right panels) of (a) $CuAlO_2$ and (b) $AgAlO_2$. HSE calculations were performed to obtain accurate band gaps and only select HSE bands are displayed. The densities of states were derived from the PBE calculations.

structure in the current work and assume that the $3R$ behaves similarly.

Table I lists the calculated and experimental values of the lattice constants, the Cu-O and Ag-O bond lengths, and the M-O (M = B, Al, Ga, In, Sc) bond lengths. For most of the compounds, the calculated results are in good comparison with the experimental values. The only exception is $CuBO_2$, for which a large discrepancy can be seen and which might be caused by the poor quality of the film samples. Indeed, given the good agreement in the other systems, these results cast some doubt on the nature of the $CuBO_2$

FIG. 4. (Color online) The projected DOS for Cu_2O, Ag_2O, and selected delafossites.

experiments. For $CuIIIO_2$ and $AgIIIO_2$ compounds (III stands for group-III elements, including B, Al, Ga, and In), the lattice constants ($a = b$ and c) increase with increasing atomic number, whereas the c/a ratio decreases. The change in the lattice parameters is consistent with the change in the M-O and Cu-O bond lengths. As shown in the table, the increasing size of the group-III atoms will weaken the M-O bonds and will lead to a longer bond length. The weakening of the M-O bonds in turn strengthens the Cu-O bond and makes it shorter. It is also important to notice that the Ag-O length is significantly larger than that of Cu-O. However, the M-O bond lengths are quite similar in both the Cu and Ag delafossites, although those of the latter are slightly larger. These bonding features will strongly affect the electronic structures of the compounds.

B. Electronic structure

We calculate the band structure and projected density of states (PDOS) for the delafossites. The PBE band gaps are significantly smaller than suggested by the available experimental results, whereas the HSE values agree well (Table II). The HSE gap for Cu_2O is 2.03 eV, which is in good agreement with the experimental value of 2.1 eV. This small direct gap leads to the absorption of a sizable amount of the visible light spectrum and prevents the use of Cu_2O as a p-type TCO. In comparison, the gaps in Cu and Ag delafossites are indirect and are typically larger than those of Cu_2O and Ag_2O, with only $CuInO_2$ as an exception. However, the gap of 1.74 eV for $CuInO_2$ is indirect, and its direct gap is 4.65 eV, which is much larger than the energy of blue light.

Although HSE significantly improves the band gap values, some delafossites still show a considerable difference between the HSE band gaps and the experimental measurements. The deficiencies may come from both the theoretical sites and the experimental sites. As a hybrid functional method that mixes the exact exchange energy and the local and semilocal functionals, HSE results may still be different from the true gaps and the discrepancy strongly varies with the materials.
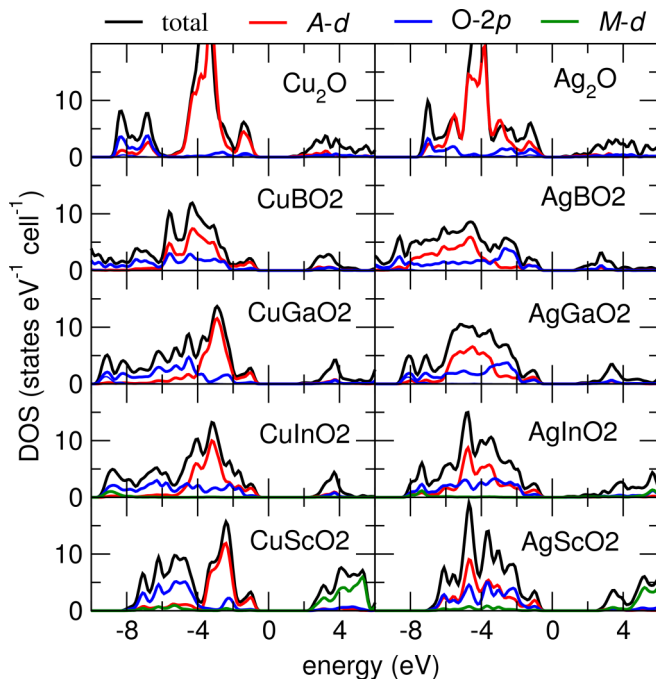
TABLE III. The calculated ionization energies and the electron affinities for Cu and Ag oxides and delafossites.

	IE (eV)			EA (eV)		
	PBE	HSE	Expt.	PBE	HSE	Expt.
Cu_2O	4.273	5.181	5.25 [44]	3.751	3.151	3.15 ± 0.1 [28,44]
$CuBO_2$	5.382	5.930		3.833	2.734	
$CuAlO_2$	4.771	5.372		2.952	1.922	
$CuGaO_2$	4.843	5.455		4.040	3.028	
$CuInO_2$	4.440	5.147		4.134	3.412	
$CuScO_2$	4.608	5.112		1.918	1.059	
Ag_2O	4.967	5.793		5.030	4.699	
$AgBO_2$	5.713	7.080		4.981	5.111	
$AgAlO_2$	5.400	6.387		3.957	3.631	
$AgGaO_2$	5.457	6.460		4.864	4.493	
$AgInO_2$	5.072	5.729		4.782	4.073	
$AgScO_2$	4.988	5.790		2.856	2.242	

These results can in principle be improved by tuning the mixing amount and the screening length, but the optimal values will be different for different compounds. In order to compare the band edge states of all delafossites at the same base, we choose to use the standard mixing parameter of 0.25 throughout our calculations. On the other hand, there are not many band gap measurements available for delafossites. Most of them are based on optical absorption spectroscopy and have considerable uncertainties. X-ray photoelectron spectroscopy measurements are available for $CuAlO_2$ and $CuScO_2$. However, the comparison of our HSE results with them is not better than with the absorption spectra.

Furthermore, Shin *et al.* measured the bandwidth of the top valence bands using x-ray emission spectroscopy (XES) [43], which can be compared to our HSE results. Their measurements found a progressive bandwidth decrease, $CuAlO_2 > CuGaO_2 > CuInO_2 > CuScO_2$. In comparison, the HSE valence bandwidths are 8.61, 8.54, 7.06, and 6.12 eV for the compounds in the same order. Except for $CuScO_2$, these values show considerable improvements while comparing with the XES spectroscopy than the previous DFT results obtained by using the semilocal functionals.

The band structures and PDOS of $CuAlO_2$ and $AgAlO_2$ are shown in Fig. 3. The PDOS of all other studied compounds are shown in Fig. 4. The states around the valence band maximum (VBM) of $CuAlO_2$ are predominantly Cu-3d states, while the O-2p states are mainly located 2–3 eV below the VBM. Conversely, the states around the VBM of $AgAlO_2$ consist of both O-2p and Ag-4d states, with the Ag-4d states also extending down to significantly lower energies. These electronic structure features affect the electronic properties of Cu and Ag delafossites, such as the effective mass and the ionization energies and electron affinities.

The VBM is located at the L point for both $CuAlO_2$ and $AgAlO_2$, although the energies of the highest VB states at the M, H, and K points are also very close to those of the VBM. In both compounds, the conduction band minimum (CBM) is located at the Γ point. We assume that the energy difference between the average electrostatic potential of the bulk material and the vacuum level is the same for both the PBE and HSE calculations because the HSE functional only makes a slight change to the ground state charge distribution. We therefore align the Kohn-Sham orbital energies at each point. As shown in Fig. 3(a), the HSE calculation for $CuAlO_2$ shifts the VBM downward and the CBM upward by almost equal amounts. These shifts result in an increased ionization energy and a decreased electron affinity. A similar trend is also found for $AgAlO_2$, however, its correction to the VBM level is more significant than that for the CBM [Fig. 3(b)].

The band structures for both compounds display large in-plane dispersions and very small dispersions in the perpendicular direction. These differences in the dispersion are consistent with the crystalline anisotropy of the delafossite structure and result in the hole mobility being much smaller in the perpendicular direction.

C. Band alignments

The positions of the band edge states are calculated using the slab model described in the Methodology section above. The calculated ionization energies (IEs) and electron affinities (EAs) are listed in Table III and are also presented schematically in Fig. 5. PBE underestimates the ionization energy of Cu_2O by about 1 eV and overestimates the electron affinity by about 0.6 eV. Therefore, the reduction of the band gap in the PBE calculations is caused by both the downward shift of the CBM and the upward shift of the VBM. On the other hand, HSE corrects most of the PBE errors and yields IE and EA values that are in good agreement with experiment. For most other compounds, HSE corrects the IE and EA results by lowering the VBM and increasing the CBM energies.

Our results are generally in good agreement with prior theoretical studies, despite the use of different models (surface slab versus superlattice) and functionals (LDA/GGA versus hybrid). For example, we found that $CuAlO_2$ and $CuScO_2$ have a staggered band alignment, i.e., they may form a type-II quantum well or superlattice. This agrees with the result of Shi *et al.* [8], although the valence band offset in that study was 0.40 eV while our result is a smaller, 0.16 eV. The band alignments across group-III Cu-based delafossites follow the same general trend as previously calculated [12]. However, in contrast to Nie *et al.*, we find that the VBM of $CuGaO_2$ is lower than that of $CuAlO_2$.
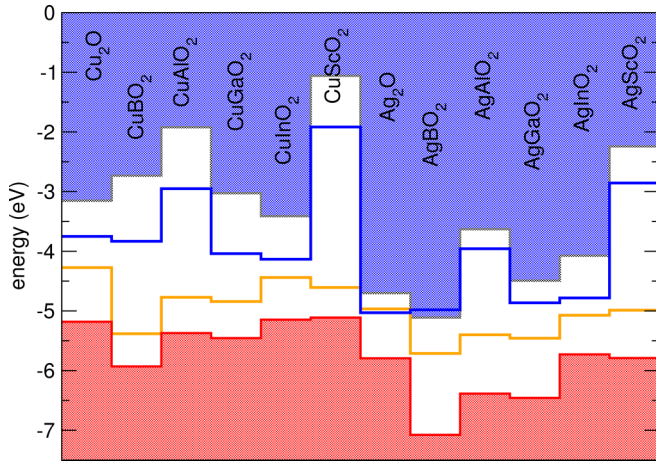
FIG. 5. (Color online) Delafossite band alignments with respect to the vacuum level. The edges of the blue and the red areas represent the positions of the CBM and the VBM calculated by the HSE functional, whereas the blue and the orange lines show the results obtained by the PBE functional.

The band alignments can reveal the propensity for n- and p-type doping of materials. Compared with Cu_2O, the VBM of the Cu delafossites varies only slightly, with the exception of $CuBO_2$. As shown in Table III and Fig. 5, $CuBO_2$ has the largest IE, and its VBM is about 0.75 eV lower than that of Cu_2O, suggesting that $CuBO_2$ is not a good p-type TCO candidate. Varying from B to In, the IE decreases in general, except that the IE of $CuGaO_2$ is about 0.08 eV higher than $CuAlO_2$. The IE of $CuInO_2$ is slightly lower than Cu_2O, suggesting a good p-type doping propensity for the material. Although the indirect band gap of $CuInO_2$ is only 1.74 eV, its direct gap at L point is as large as 4.65 eV. Furthermore, $CuScO_2$ has an IE of 5.11 eV, which is 0.07 eV lower than Cu_2O. Its band gap is as large as 4.05 eV, making it well qualified as a potential p-type TCO.

The VBM position in the Ag delafossites shows a similar trend as the Cu delafossites, i.e., the VBM shift upward with an increasing atomic number of the group-III element. Among all the related compounds, $AgBO_2$ has the lowest VBM. $AgInO_2$ has a desirable VBM position since its IE is 5.73 eV, close to that of Ag_2O. Although its indirect band gap is only 1.66 eV, $AgInO_2$ possesses a direct gap of 2.26 eV, which, similar to $CuInO_2$, is large enough to transmit green light. In addition, $AgScO_2$ has a gap of 3.55 eV and its IE is the about the same as Ag_2O. Generally speaking, the VBMs of silver oxide and the Ag delafossites are lower than those of the analogous Cu compounds. This difference is a result of a greater stabilization of the Ag-4d state than the Cu-3d state. This smaller IE leads to a better p-type doping propensity that is important for the use of Cu delafossites as TCOs.

The delafossite structure is a mixture of the Cu_2O structure and the M_2O_3 structure, stacked in alternating layers. Many structural features, such as the linear O-Cu-O and the MO_6 octahedra, are preserved in the delafossite structure. Geometric features of the native compounds are modified by the mixture, and the electronic properties of delafossites depend on the interplay between the Cu_2O and the M_2O_3 layers. As shown
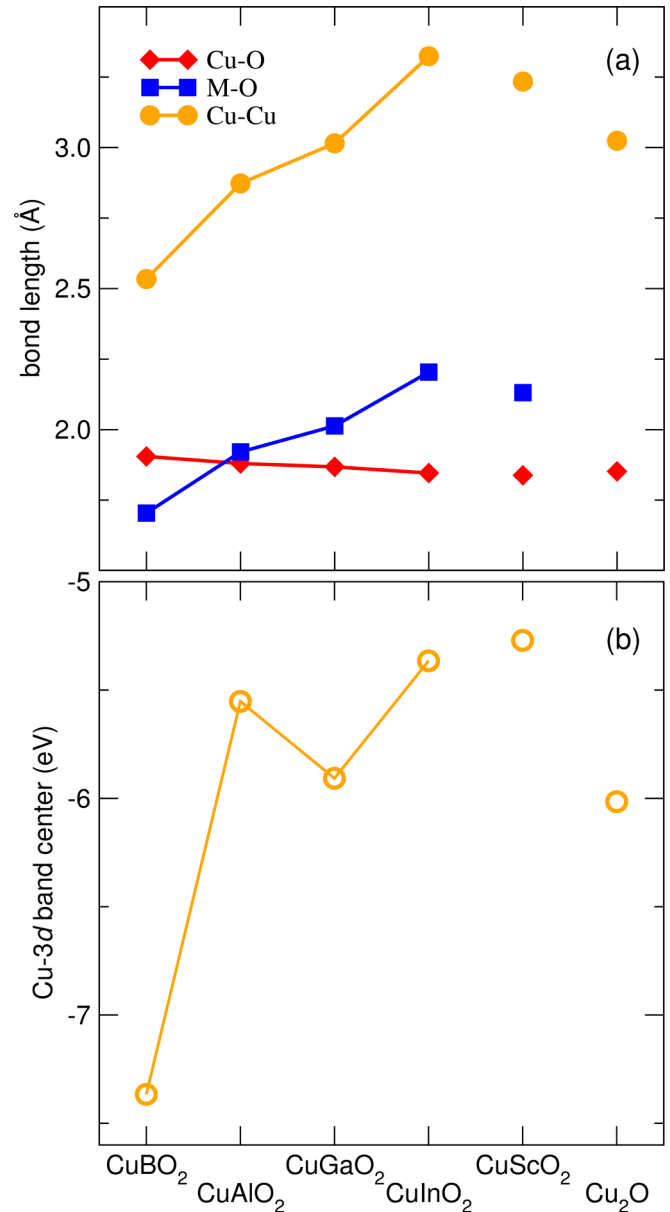

FIG. 6. (Color online) Compositional trends in (a) bond lengths and (b) position of the Cu-3d band center.

in Fig. 6(a), the Cu-O bond length differs only slightly from Cu_2O and Cu delafossites. The M-O bond length varies greatly among the delafossites, ranging from the smallest for $CuBO_2$ (1.704 Å by PBE) to the largest for $CuInO_2$ (2.204 Å by PBE). The M-O bond lengths are slightly compressed in comparison to those in the native oxides. For example, the average Al-O bond length in Al_2O_3 is 1.943 Å, whereas in $CuAlO_2$ it is 1.921 Å.

Among all the geometric features, the most change is seen in the Cu-Cu distance. As shown in Fig. 6(a), the nearest-neighbor Cu-Cu distance varies from 2.534 Å for $CuBO_2$ to 3.324 Å for $CuInO_2$. The modulation of the Cu-Cu distance significantly affects the coupling between the 3d orbitals at neighboring Cu atoms and changes the width of the 3d bands. A shorter Cu-Cu distance leads to broader 3d bands, and thus they are broadest in $CuBO_2$, covering an energy range of about

10 eV (Fig. 4). Oppositely, Cu_2O has the most narrow $3d$ bands, partially due to its larger Cu-Cu distance and partially due to the misalignment of the $3d$ orbitals on neighboring Cu atoms.

The broadening of the $3d$ bands in the Cu delafossites should, in principle, cause an upward shift in the VBM energy; however, our calculations show the opposite behavior, with the VBM increasing with the increasing size of the M atom. We explain this by examining the center of the Cu-$3d$ bands in Cu_2O and the Cu delafossites. As shown in Fig. 6(b), the Cu-$3d$ band center rises as the size of M increases. This leads the $CuBO_2$ $3d$ band center to be about 5 eV lower than that of $CuInO_2$, consistent with our IE results. The center of the Cu-$3d$ bands in $CuScO_2$ and Cu_2O is 3–4 eV below $CuInO_2$. However, since the $3d$ bands are significantly narrower, the VBM energies are comparable with those of $CuInO_2$.

IV. CONCLUSION

In summary, we systematically studied the atomic and electronic structures of a series of Cu and Ag delafossites using the first principles DFT method with hybrid functionals featuring a screened exchange. The band alignments (the ionization energies and the electron affinities) are calculated by aligning the average electrostatic potential in the bulk region of the compounds and the vacuum region in a slab model.

A nonpolarized orientation was chosen to minimize artifacts caused by the surface dipoles. The calculated IE and EA values for Cu_2O are in excellent agreement with the experimental values. We found that the VBM energies of delafossites do not differ significantly from the native oxides, except for $CuBO_2$ and $AgBO_2$. Their low VBM indicates the difficulty of p-type doping in these materials. On the other hand, $CuAlO_2$, $CuGaO_2$, and especially $CuScO_2$ are good candidates for p-type TCOs. The compositional variation of the VBM energy is the combined result of both the $3d$-band widths and centers, which are controlled by structural features such as the Cu-Cu or Ag-Ag distances. At the end, we would also like to emphasize that although the study of the band edge states can provide a good indication of the doping propensity of the semiconductor materials, the nature of the defect states and their formation can only be revealed by direct defect calculations. Although the methods are well developed for such calculations, a full scale first principles investigation requires a large amount of resources for one material and can hardly be done across an entire family of materials.

[1] G. Thomas, Nature (London) **389**, 907 (1997).

[2] B. J. Ingram, G. B. Gonzalez, D. R. Kammler, M. I. Bertoni, and T. O. Mason, J. Electroceramics **13**, 167 (2004).

[3] H. Raebiger, S. Lany, and A. Zunger, Phys. Rev. B **76**, 045209 (2007).

[4] H. Kawazoe, M. Yasukawa, H. Hyodo, M. Kurita, H. Yanagi, and H. Hosono, Nature (London) **389**, 939 (1997).

[5] H. Yanagi, S. Inoue, K. Ueda, H. Kawazoe, H. Hosono, and N. Hamada, J. Appl. Phys. **88**, 4159 (2000).

[6] Y. J. Shin, J. P. Doumerc, P. Dordor, M. Pouchard, and P. J. Hagenmuller, Solid State Chem. **107**, 194 (1993).

[7] D. O. Scanlon and G. W. Watson, J. Mater. Chem. **21**, 3655 (2011).

[8] L.-J. Shi, Z.-J. Fang, and J. Li, J. Appl. Phys. **104**, 073527 (2008).

[9] D. O. Scanlon, K. G. Godinho, B. J. Morgan, and G. W. Watson, J. Chem. Phys. **132**, 024707 (2010).

[10] R. Seshadri, C. Felser, K. Thieme, and W. Tremel, Chem. Mater. **10**, 2189 (1998).

[11] H. C. Kandpal and R. Seshadri, Solid State Sci. **4**, 1045 (2002).

[12] X. Nie, S.-H. Wei, and S. B. Zhang, Phys. Rev. Lett. **88**, 066405 (2002).

[13] A. Klein, C. Körber, A. Wachau, F. Säuberlich, Y. Gassenbauer, S. P. Harvey, D. E. Proffit, and T. O. Mason, Materials **3**, 4892 (2010).

[14] T. Dietl, H. Ohno, F. Matsukura, J. Cibert, and D. Ferrand, Science **287**, 1019 (2000).

[15] S. Sanvito, P. Ordejon, and N. A. Hill, Phys. Rev. B **63**, 165206 (2001).

[16] D. O. Scanlon, C. W. Dunnill, J. Buckeridge, S. A. Shevlin, A. J. Logsdail, S. M. Woodley, C. R. A. Catlow, M. J. Powell, R. G. Palgrave, I. P. Parkin *et al.*, Nat. Mater. **12**, 798 (2013).

[17] A. Kirfel and K. D. Eichhorn, Acta Crystallogr. Sect. A **46**, 271 (1990).

[18] M. Snure and A. Tiwari, Appl. Phys. Lett. **91**, 09123 (2007).

[19] B. U. Koehler and M. Jansen, Z. Anorg. Allg. Chem. **543**, 73 (1986).

[20] O. Garlea, P. Bordet, C. Darie, O. Isnard, and R. Ballou, J. Phys.: Condens. Matter **16**, S811 (2004).

[21] A. Kato and Y. Anju, J. Am. Ceram. Soc. **55**, 25 (1972).

[22] G. Brachtel and M. Jansen, Cryst. Struct. Commun. **10**, 173 (1981).

[23] B. U. Koehler and M. Jansen, J. Solid State Chem. **71**, 566 (1987).

[24] V. Dietrich and M. Jansen, Z. Naturforsch., B: Anorg. Chem., Org. Chem. **66**, 227 (2011).

[25] A. Pabst, Am. Mineral. **31**, 539 (1946).

[26] W. J. Choyke, D. R. Hamilton, and L. Patrick, Phys. Rev. **133**, 1163 (1964).

[27] W. R. L. Lambrecht, S. Limpijumnong, S. N. Rashkeev, and B. Segall, Phys. Status Solidi B **202**, 5 (1997).

[28] S. Brahms, S. Nikitine, and J. P. Dahl, Phys. Lett. **22**, 31 (1966).

[29] D. O. Scanlon, A. Walsh, and G. W. Watson, Chem. Mater. **21**, 4568 (2009).

[30] D. J. Aston, D. J. Payne, A. J. H. Green, R. G. Egdell, D. S. L. Law, J. Guo, P. A. Glans, T. Learmonth, and K. E. Smith, Phys. Rev. B **72**, 195115 (2005).

[31] K. Ueda, T. Hase, H. Yanagi, H. Kawazoe, H. Hosono, H. Ohta, M. Orita, and M. Hirano, J. Appl. Phys. **89**, 1790 (2001).

[32] J. W. Lekse, M. K. Underwood, J. P. Lewis, and C. Matranga, J. Phys. Chem. C **116**, 1865 (2012).

[33] H. Yanagi, T. Hase, S. Ibuki, K. Ueda, and H. Hosono, Appl. Phys. Lett. **78**, 1583 (2001).

[34] S. Gilliland, J. Sánchez-Royo, J. Pellicer-Porres, A. Segura, A. Muñoz, P. Rodríguez-Hernández, and J. López-Solano, Thin Solid Films **516**, 1431 (2008).

[35] H. Hiraga, T. Makino, T. Fukumura, A. Ohtomo, and M. Kawasaki, Appl. Phys. Lett. **95**, 211904 (2009).

[36] C. Tseng, J. Hsieh, and W. Wu, Thin Solid Films **519**, 5169 (2011).

[37] S. Ouyang, H. Zhang, D. Li, T. Yu, J. Ye, and Z. Zou, J. Phys. Chem. B **110**, 11677 (2006).

[38] S. Ouyang, Z. Li, Z. Ouyang, T. Yu, J. Ye, and Z. Zou, J. Phys. Chem. C **112**, 3134 (2008).

[39] W. C. Sheets, E. S. Stampler, M. I. Bertoni, M. Sasaki, T. J. Marks, T. O. Mason, and K. R. Poeppelmeier, Inorg. Chem. **47**, 10741 (2008).

[40] Y. Maruyama, H. Irie, and K. Hashimoto, J. Phys. Chem. B **110**, 23274 (2006).

[41] K. A. Vanaja, R. S. Ajimsha, A. S. Asha, and M. K. Jayaraj, Appl. Phys. Lett. **88**, 212103 (2006).

[42] S. Ouyang, N. Kikugawa, D. Chen, Z. Zou, and J. Ye, J. Phys. Chem. B **113**, 1560 (2009).

[43] D. Shin, J. S. Foord, D. J. Payne, T. Arnold, D. J. Aston, R. G. Egdell, K. G. Godinho, D. O. Scanlon, B. J. Morgan, G. W. Watson *et al.*, Phys. Rev. B **80**, 233105 (2009).

[44] J. Caballero-Briones, M. Artés, I. Díez-Pérez, P. Gorostiza, and F. Sanz, J. Phys. Chem. C **113**, 1028 (2009).